Analyst

ROYAL SOCIETY OF CHEMISTRY

COMMUNICATION

View Article Online
View Journal | View Issue



Cite this: *Analyst*, 2022, **147**, 3415

Received 26th April 2022,
Accepted 1st June 2022

DOI: 10.1039/d2an00712f

rsc.li/analyst



# Spatially-extended 3D magnetic DNA nanodevice-based split-type photoelectrochemical strategy for sensitive and reliable miRNA detection in cancer cells†

Hui Yuan,[a] Jiuming Sun,[a] Qi Zhang,[a] Mingyue Chu,[a] Guiguang Cheng,[b] Xia Li *[a] and Qingwang Xue *[a]

**Highly sensitive and reliable PEC detection of miRNAs still faces some challenges like the inaccuracy caused by coexisting interferences in the PEC system. Herein, we developed a split-type "turn-off" PEC biosensor based on spatially-extended 3D magnetic DNA nanodevices with high-order DNA amplifiers for sensitive detection of miRNAs in cancer cells.**

MicroRNA (miRNA) performs crucial functions in feedback mechanisms by safeguarding key biological processes including the regulation of gene expression and attenuation of apoptosis, where its expression levels in cancer cells are closely related to malignant diseases. Recent studies have demonstrated that cancer-specific fingerprints of miRNAs can provide important information about tumor initiation, the progression of invasion, and metastasis. Interestingly, intracellular miRNA has emerged as a promising genetic marker for cancer progression and prognosis.[1] These findings have fueled the need to develop highly sensitive and reliable detection methods for miRNA in cancer cells to obtain information on the progress of malignancy and better guidance in practical clinical applications. Therefore, the development of strategies for simple, sensitive, and robust quantitative detection of miRNA in cancer cells has become imperative.

Recently, some engaging strategies have been proposed for the detection of miRNA in biological samples, including fluorescence,[2] electrochemical,[3,4] surface plasmon resonance,[5] ECL[6] and photoelectrochemical (PEC).[7] In particular, the PEC technique exhibits unique merits of low background and high sensitivity resulting from the separated optical excitation and signal readout.[8–12] Typically, most PEC biosensors involve the interfacial confinement of DNA probes on the photoelectrode, followed by passivation with a blocking reagent that backfills the unoccupied space and forces the probe to adopt a vertical direction for target recognition.[13–16] Unfortunately, the binding of biomolecules on photoelectrodes may inevitably cause the weakening of the photocurrent signal due to their steric hindrance effect on mass transfer and target accessibility, and the interference in light absorption of photovoltaic substrates. Moreover, tedious electrode assembly and cleaning procedures reduce the accuracy and stability of the PEC sensor.[17–19] In order to overcome the above bottlenecks, a variety of split PEC detection methods have been developed in recent years, which can well avoid the interference between biometric identification and PEC detection system.[20] To improve the sensitivity, various enzyme/nucleic acid amplification circuits were introduced into the homogeneous PEC system.[19,21] Despite these substantial achievements in sensitivity, there are still some challenges of concern. For example, target recognition and signal output were carried out in the same solution, and the coexisting enzyme or nucleic acid substrate was susceptible to being adsorbed to the electrode surface, resulting in electrode contamination. In addition, the coexisting reducing components in biological samples ($H_2O_2$ or dopamine) will compete with the electron donor, leading to an unpredictable photocurrent response, thereby affecting the accuracy.[22] Thus, an unconventional split-type PEC strategy is still urgently desired in biological sample analysis.

3D magnetic DNA nanodevices are emerging as potential alternatives to the strategy of constructing split-type sensors due to their attractive attributes associated with highly efficient removal of coexisting interference substances.[17] This platform can also permit concentrating on the substrate probe in the nanospace to improve reaction efficiency and amplification ability.[23] For example, Li *et al.* developed a split-type PEC biosensor by introducing superparamagnetic $Fe_3O_4$@$SiO_2$ to control the load of a CdTe-modified DNA signal for sensitive detection of miRNA-122.[24] Recently, our group developed a split-type digital quantitative aptasensor by using superparamagnetic $Fe_3O_4$ to control the load of an invertase–DNA conju-

[a]*Department of Chemistry, Liaocheng University, Liaocheng, 252059 Shandong, China. E-mail: lixia@lcu.edu.cn, xueqingwang1983@163.com; Fax: +86-635-8239001; Tel: +86-635-8239001*

[b]*Faculty of Agriculture and Food, Kunming University of Science and Technology, Kunming, China*

† Electronic supplementary information (ESI) available: Experimental details and additional figures. See DOI: https://doi.org/10.1039/d2an00712f

gate for on-the-spot detection of antibiotics.[25] Although these magnetic DNA nanodevices can be obtained by one-step hybridization with CdTe-modified DNA or an invertase–DNA conjugate onto the surface of $Fe_3O_4$ nanoparticles, some limitations remain. For example, the size of CdTe and invertase were both larger than 3 nm, which is comparable to small $Fe_3O_4$ probes.[24] In this sense, the amount of coupling capture of DNA was significantly reduced due to the interface hindrance effect. Moreover, in the one-step hybridization mode, the loaded DNA is only confined to the limited surface of magnetic $Fe_3O_4$ nanoparticles, which cannot be extended to three-dimensional space, thus limiting its removal performance and impairing the sensitivity for detection. Currently, the application of 3D DNA nanodevices in PEC biosensing is still in its infancy. Therefore, more efforts should be devoted to this area to meet the demand for high sensitivity analysis of trace miR-21 in complex biological samples.

Herein, we developed a facile split-type "turn-off" PEC biosensor based on spatially-extended 3D magnetic DNA nanodevices with high-order DNA scaffold amplifiers for the sensitive and selective detection of miRNAs. A highly amplified signal and low background are achieved by a high-order DNA scaffold made by rolling circle amplification (RCA) self-assembly and magnetic separation. In this strategy, a padlock probe (P-circle, green yellow) is designed to be complementary to the target miR-21 (light yellow) at its 5′- and 3′-terminals. In the presence of miR-21, the formed RNA/DNA complex between the padlock probe and miR-21 served as an engaging primer to initiate the RCA process, generating abundant single-strand DNA (RCA–DNA). The RCA–DNA served as the framework, which was designed to include the anchoring sequence for one short functional DNA (biotin-P1, red) and two short unmodified DNAs (P2, purple; P3, green). Through periodic binding with the bio-P1 (biotin-modified P1), P2 and P3, respectively, the long RCA–DNA can be folded and self-assembled into higher-order superstructures (Fig. S1†). Benefitting from the strong interaction of biotin–streptavidin and the multivalency of streptavidin molecules (one streptavidin binds four biotins), multiple higher order DNA scaffolds can be anchored to streptavidin-modified $Fe_3O_4$ (strep-MB), forming 3D magnetic DNA. In this sense, the loaded DNA scaffold was not only limited to the surface of magnetic $Fe_3O_4$ nanoparticles, but also can be extended into the three-dimensional space (Fig. 1A). In this case, by transferring the 3D magnetic DNA nanodevice to an MB solution, the carried higher-order DNA scaffold amplifier can be used as a huge container to load MB through its abundant guanine bases and double helix grooves. After magnetic separation, the remaining pure MB molecules result in a reduced photocurrent signal, which is directly inversely proportional to miRNA with extremely high sensitivity (Fig. 1B). In contrast, in the absence of target miR-21, the proposed RCA is blocked; the RCA–DNA products and the spatially extended 3D magnetic DNA nanodevices cannot be generated, resulting in no obvious change in photocurrent. In our system, the RCA-based high-order DNA scaffold assembled 3D magnetic DNA nanodevice expanded the scope of space and overcame the

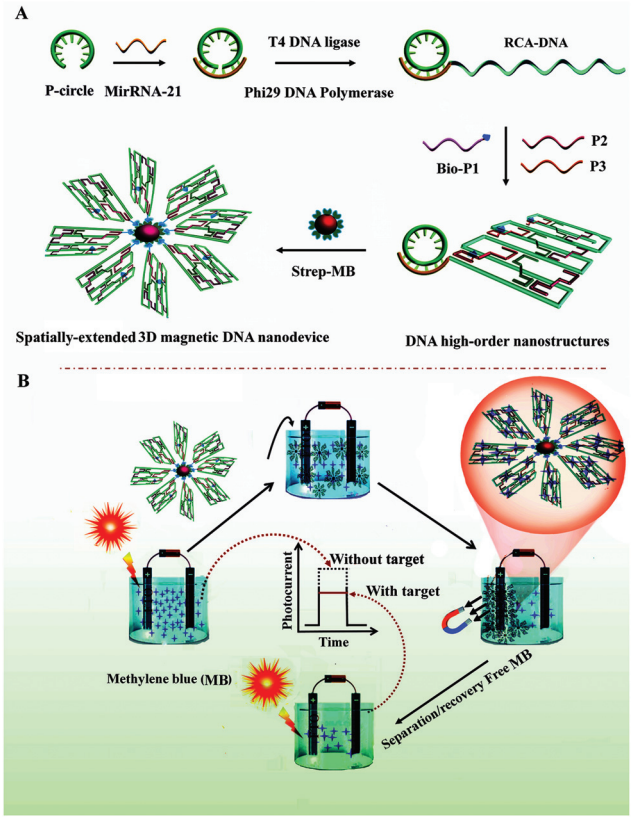


**Fig. 1** Schematic illustration of the spatially-extended 3D magnetic DNA nanodevice-based split-type photoelectrochemical strategy for sensitive and reliable miRNA detection. (A) Target recognition process; (B) PEC signal output process.

spatial hindrance effect on magnetic nanoparticles, thus enhancing the DNA load capacity and MB removal ability and further increasing signal amplification. Target recognition and signal output occur in two different reaction pools, avoiding interference of biological sample components to the PEC response and guaranteeing reliability. The split-type "turn-off" PEC sensor can achieve remarkable detection limits (2.4 fM) and eliminate the instability caused by the PEC system. Significantly, the proposed strategy was demonstrated with high selectivity and capability of detecting miR-21 in the total RNA samples extracted from different cells. Given the need for high performance miRNA analysis in cancer cells, the strategy shows promise in its application to complex biological matrices.

To verify the feasibility of the 3D magnetic DNA nanodevice-based split-type PEC strategy for miR-21 detection, we performed electrophoretic analysis using 2% agarose gel in a TAE buffer (Fig. 2A). In the presence of miR-21, the band of the product (lane 4) migrated slower than the padlock (lane 2), resulting from the miR-21 mediated RCA process with the designed DNA structures. Notably, with the addition of three primers (P1, P2, and P3, lanes 5–7), a discrete band of different mobility was observed while the bands of low molecular weight corresponding to the three short primers disappeared (lane 8), suggesting the formation of high-order DNA

 

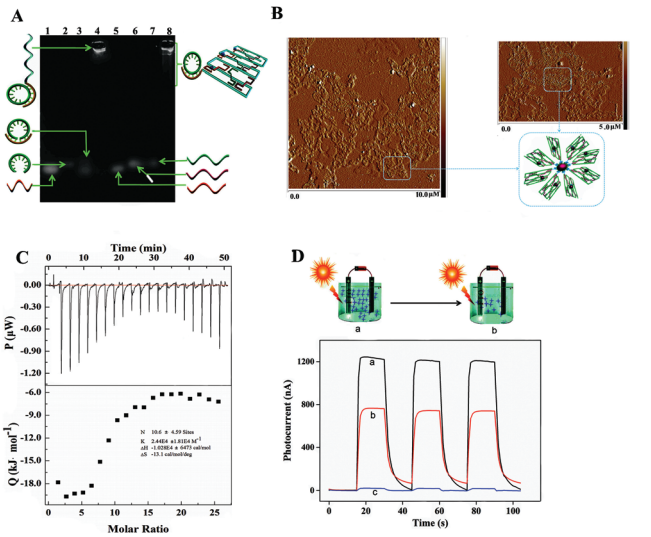


**Fig. 2** (A) Agarose gel analysis of high-order DNA scaffolds. Lane 1: miR-21; lane 2: padlock; lane 3: padlock + miR-21; lane 4: miR-21 + padlock strand + DNA polymerase; lane 5: P1; lane 6: P2; lane 7: P3; lane 8: miR-21 + padlock + P1 + P2 + P3 + DNA polymerase. (B) AFM image of 3D magnetic DNA nanodevices. (C) Thermodynamic parameters corresponding to the inclusion complex between highly folded DNA and MB. (D) PEC response of the proposed PEC sensor in the absence of the miR-21 (a) and in the presence of the miR-21 (b).

nanostructures. In order to further explore the distribution of high-order DNA nanostructures on the surface of magnetic nanoparticles, bio-P1, P2, P3 and streptavidin-modified $Fe_3O_4$ (strep-MB) were introduced into the RCA product system in sequence and the products were further characterized by AFM. As shown in Fig. 2B, magnetic nanoparticles were surrounded by highly dense high-order DNA nanostructures, which was in accordance with the agarose gel electrophoresis results. This indicated that the RCA mediated high-order DNA scaffolds enable loaded DNA probes not only to be confined to the surface of magnetic $Fe_3O_4$ nanoparticles but also to be extended into the surrounding space.

To test whether the high-order DNA scaffolds have the ability to capture free MB, after transferring the high-order DNA scaffolds into the pure MB solution, a photochemical analysis was performed (Fig. S3†). The proposed PEC platform employs free MB as the photochemical signal reporter and a negatively charged FTO electrode as the working electrode. A reduced PEC response can be successfully achieved based on the diffusivity difference between free MB molecules and MB molecules embedded within high-order DNA scaffolds, which was similar to the previous system with dsDNA for capturing MB.[26,27] More interestingly, in the above free MB and coexisting MB/DNA scaffoldssituation, the repeated photocurrent tends to rise slowly as the test time goes on (Fig. S3†). To further explore this process, the stoichiometry and binding energy of the interaction between MB and high-order DNA scaffolds were studied by ITC experiments at 310.15 K (Fig. 2C). The $N$ value was 10.6 ± 4.59, suggesting that each "boxcar" of high-order DNA can load about 6–14 MB molecules, indicating that it has a high ability to capture MB. In this multimodal bonding process, where free MB and MB/DNA complexes coexist, the electronegativity of the complex decreases significantly, which may overcome electrostatic repulsion and allow diffusion to the electrode surface, thus interfering with the original stability. Moreover, with continuous PEC detection, the binding dynamic equilibrium of MB/DNA might be influenced by the surrounding environment and lead to imperfect reliability. Therefore, in the PEC system, where the substrate probes and signal reporters coexist, mutual interference cannot be avoided.

To eliminate mutual interference, a target recognition and signal output spatial partition based PEC approach was proposed. As shown in Fig. 2D, when the target miR-21 was present, a significantly reduced photoelectric signal was observed compared to that of the initial MB solution. This suggests that the target sequence can be hybridized with a lock-like probe, initiating an RCA process that locks onto one biotin DNA and two short unmodified DNAs. The resulting periodic DNA/DNA hybrids can self-assemble in a high-order folded manner and then bind to streptavidin magnetic nanobeads to form space-expanded 3D magnetic DNA nanodevices through avidin–biotin conjugation. After transferring them into the pure MB solution, a large amount of MB was embedded into magnetic DNA nanodevices and then removed by magnetic separation. Therefore, the concentration of MB was drastically reduced and resulted in a photocurrent decrease in a proportional manner. In contrast, in the control system without miR-21, there was no distinct photocurrent attenuation compared to that in the initial MB solution (Fig. 2D). This indicated that in the absence of miR-21, the padlock probe could not circulate and trigger the subsequent RCA process, thus preventing the formation of periodic DNA/DNA hybrids. In this case, by transferring magnetic DNA nanodevices to a pure MB solution, it is difficult to remove MB because it only carries P1, resulting in a lack of MB insertion sites. All results testify to the operational feasibility of the designed split-type PEC platform.

To improve the operational performance of the as-proposed split-type PEC assay, the experimental conditions should be carefully optimized (Fig. S4†). Under optimal experimental conditions, the as-proposed PEC platform was used to quantitatively determine miR-21 with different concentrations. Fig. 3A depicts the photocurrent responses of the split-type PEC sensor after incubation with target miR-21. Evidently, the photocurrents decreased as the miR-21 concentration increased from 0 fM to 1 μM, which is attributed to the drastically reduced presence of MB induced by the powerful target-triggered removal of MB/DNA complexes. Moreover, the photocurrent change ($\Delta I$, the difference between the photocurrents in the presence and absence of the miR-21) exhibits a good linear correlation with the logarithm of the miR-21 concentration ranging from 10 fM to 1 μM (Fig. 3B). The corresponding linear correlation equation is $\Delta I = 76 \lg C_{\text{miR-21}} - 49$ and the correlation coefficient ($R^2$) is 0.9889, where $\Delta I$ is the photocurrent change (nA) and $C$ is the miR-21 concentration

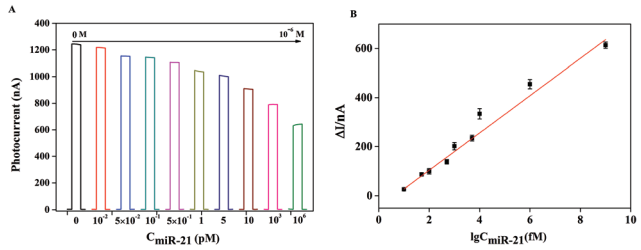


Fig. 3 (A) Photocurrent values at different concentrations of miR-21. (B) The photocurrent changes at miR-21 concentrations ranging from 10 fM to1 μM were used to fit the linear relationship. The error bars represent the standard deviation of three repetitive measurements.

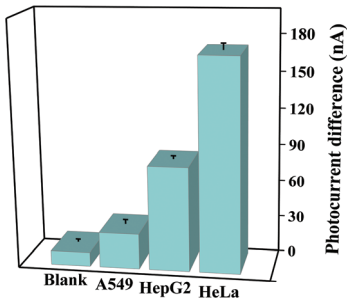


Fig. 5 Detection of miR-21 in different cell lysates (about $8 \times 10^5$ cells). The concentration of the padlock probe is 1 μM. The error bars represent the standard deviation of three repetitive measurements.

(fM). The detection limit was recorded as 2.4 fM ($S/N$ of 3), which was comparable or superior to some reported analysis strategies toward miR-21 (Table S2†).

To assess the reliability of the results in this split-type PEC strategy, the precision and reproducibility were explored by calculating the relative standard deviation (RSD) of intra- and inter-assays. Three concentrations of miR-21 (0.4 pM, 0.4 nM and 0.4 μM) within the linear range were chosen for the test. Intra-assay precision and inter-assay precision for three parallel determinations of the miR-21 sample were performed on the same day and after three days, respectively (Fig. 4B). For miR-21 detection, the RSD of the intra-assay precision were 0.46%, 0.62% and 0.47% and the RSD of the inter-assay precision were 1.39%, 3.45% and 3.15%, respectively. These results indicated that the as-proposed PEC sensor possessed satisfactory precision and reproducibility.

Specificity is an essential indicator of a sensing platform. Due to the highly sequential homological similarity between family members, distinguishing the difference between miRNA family members remains a great challenge. To evaluate the specificity of the split-type PEC sensing platform, sequences such as miR-155, miR-141 and let-7b were chosen as possible distractors (Fig. 4A). The photocurrent responses of several miRNAs, including miR-155, miR-141 and let-7b were separately measured at the same concentration. As displayed in Fig. 4C, only miR-21 induced a dramatic enhancement of $\Delta I$ while other interfering miRNAs showed negligible changes. These results suggested that this strategy displayed high selectivity for the detection of miR-21.

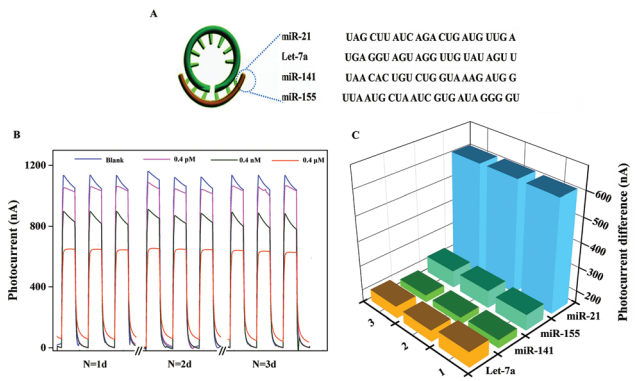


Fig. 4 Specificity and stability of the split-type PEC biosensor. (A) Sequences of different types of miRNAs. (B) The intra-assay and inter-assay precision under different miR-21 concentrations. (C) Photocurrent responses of the biosensor for different types of miRNAs: miR-21 (1 μM), let-7a (10 μM), miR-141 (10 μM), and miR-155 (10 μM).

We further examined the application of the split-type PEC strategy using real samples, namely miRNA-21 from cervical cancer cells (HeLa), human hepatic cancer cells (HepG2) and human non-small cell lung cancer cells (A549), which were put into practice. As shown in Fig. 5, upon analysing the samples containing lysates from the above cells, this system exhibits a higher photocurrent response to HepG2 cells and HeLa cells and a lower photocurrent response to A549 cells, which is consistent with previous reports.[28,29] These satisfactory results well demonstrated that this split-type PEC biosensor has good potential to detect miRNAs from various cancer cells in early diagnostics.

In summary, a sensitive and reliable split-type PEC biosensor was proposed based on spatially-extended 3D magnetic DNA nanodevices with high-order DNA scaffold amplifiers mediating a "zero mutual interference" protocol. In our system, target recognition and signal output occur in two different reaction pools, avoiding the interference from biological sample components in the PEC response, thus ensuring reliability. The RCA-based high-order DNA scaffold assembled 3D magnetic DNA nanodevice expanded the scope of space and overcame the spatial hindrance effect on magnetic nanoparticles, thus enhancing DNA load capacity and MB removal ability and further increasing signal amplification. The split-type "turn-off" PEC sensor can produce a high contrast PEC signal and a low detection limit of 2.4 fM for the target miR-21. Importantly, the strategy was successfully used to assay the expression levels of miR-21 in HeLa, HepG2 and A549 cells, demonstrating that this approach holds potential for the sensitive detection of low-abundance biomarkers in complex biological matrices.

## Authorship contribution statement

Hui Yuan: Conceptualization and writing – original draft. Jiuming Sun: Data curation and formal analysis. Qi Zhang:

Investigation and methodology. Mingyue Chu: Project administration. Guiguang Cheng: Resources, software, and supervision. Xia Li: Writing – review and editing. Qingwang Xue: Writing – review and editing.

All cells were obtained from Cobioer Biosciences Co. Ltd (Nanjing, China).

## Conflicts of interest

There are no conflicts to declare.

## Acknowledgements

This project was financially supported by the Natural Science Foundation of China (21675072 and 21305058), the Natural Science Foundation of Shandong Province (ZR2019MB068 and ZR2021QE167), and the Young Innovative Talents Introduction & Cultivation Program for Colleges and Universities of Shandong Province: Innovative Research Team on Biomedical Sensing and Food Safety Research.

## Notes and references

1 M. Nicholls, *Eur. Heart J.*, 2017, **38**, 1358.
2 Z. Shi, J. Johnson and M. Stack, *J. Oncol.*, 2012, **2012**, 1.
3 X. Zhang, Z. Yang, Y. Chang, M. Qing, R. Yuan and Y. Chai, *Anal. Chem.*, 2018, **90**, 9538.
4 H. Maleh, Y. Orooji, F. Karimi, M. Alizadeh, M. Baghayeri and J. Rouhi, *Biosens. Bioelectron.*, 2021, **184**, 113252.
5 Y. Gu, J. Song, M. Li, T. Zhang, W. Zhao, J. Xu, M. Liu and H. Chen, *Anal. Chem.*, 2017, **89**, 10585.
6 T. Gao, J. Zhang, J. Wen, X. Yang, H. Ma, D. Cao and D. Jiang, *Anal. Chem.*, 2020, **92**, 1268.
7 T. Wu, M. Gui, Y. Cao, Y. Zhang, Z. Zheng, G. Xiao and H. Li, *Sens. Actuators, B*, 2022, **357**, 131395.
8 J. Shu and D. Tang, *Anal. Chem.*, 2020, **92**, 363.
9 J. Wu and Z. Liu, *TrAC, Trends Anal. Chem.*, 2020, **133**, 116089.
10 W. Zhao, J. Xu and H. Chen, *Chem. Rev.*, 2014, **114**, 7421.
11 R. Yang, K. Zou, Y. Li, L. Meng, X. Zhang and J. Chen, *Anal. Chem.*, 2018, **90**, 9480.
12 T. Liu, M. Gu, Y. Dong and G. Wang, *Anal. Chim. Acta*, 2021, **1182**, 338945.
13 F. Li, Y. Zhou, H. Yin and S. Ai, *Biosens. Bioelectron.*, 2020, **166**, 112476.
14 L. Li, Y. Zhang, Z. Yan, M. Chen, L. Zhang, P. Zhao, *et al.*, *ACS Sens.*, 2020, **5**, 1428.
15 Y. Zhao, J. Xiang, H. Cheng, X. Liu and F. Li, *Biosens. Bioelectron.*, 2021, **194**, 113581.
16 J. Wu, W. Lv, Q. Yang, H. Li and F. Li, *Biosens. Bioelectron.*, 2021, **171**, 112707.
17 (*a*) Q. Ding, M. Zhu, H. Deng, R. Yuan and Y. Yuan, *Biosens. Bioelectron.*, 2021, **184**, 113227; (*b*) X. Zhang, Y. Yin, S. Du, L. Kong, Y. Chai, Z. Li and R. Yuan, *Anal. Chem.*, 2021, **93**, 13952.
18 C. Sun, M. Liu, H. Sun, H. Lu and G. Zhao, *Biosens. Bioelectron.*, 2019, **140**, 111352.
19 (*a*) X. Liu, Y. Zhao and F. Li, *Biosens. Bioelectron.*, 2021, **173**, 112832; (*b*) J. Chang, L. Yu, H. Li and F. Li, *Sens. Actuators, B*, 2022, **352**, 131021.
20 Y. Yu, Y. Fu, K. Xiao, X. Zhang, C. Du and J. Chen, *Anal. Chim. Acta*, 2022, **1195**, 339456.
21 X. Zhang, L. Han, L. Yu, X. Wang, Y. Ling and N. Li, *ACS Appl. Mater. Interfaces*, 2021, **13**, 15881.
22 P. A. Fritz, P. Zhang, T. Bruschinski, S. Sahin, L. Smet, M. Chan-Park, R. Boom and C. Schroën, *Sep. Purif. Technol.*, 2020, **250**, 117195.
23 C. Huang, Y. Liu, Y. Sun, F. Wang, S. Ge and J. Yu, *ACS Appl. Mater. Interfaces*, 2021, **13**, 35389.
24 J. Li, X. Weng, F. Mo, M. Han and H. Li, *Anal. Chem.*, 2020, **92**, 15145.
25 X. Liu, X. Li, L. Jia, G. Cheng, D. Leong and Q. Xue, *Chem. Commun.*, 2020, **56**, 12628.
26 F. Mo, M. Han, X. Weng, Y. Zhang, J. Li and H. Li, *Anal. Chem.*, 2021, **93**, 1764.
27 T. Liu, M. Gu, Y. Dong and G. Wang, *Anal. Chim. Acta*, 2021, **1182**, 338945.
28 S. Xu, Y. Chang, Z. Wu, Y. Li, R. Yuan and Y. Chai, *Biosens. Bioelectron.*, 2020, **149**, 111848.
29 X. Zhang, Y. Yin, S. Du, L. Kong, Y. Chai, Z. Li, *et al.*, *Anal. Chem.*, 2021, **93**, 13952.